Optimization under Uncertainty using Adjoint Solver and RBF Morph

G. Petrone, D.C. Hill and M.E. Biancolini

Abstract This paper presents an industrial approach to optimization under uncertainty where the design variables and the uncertainties are handled by two different optimization modules of ANSYS Fluent, respectively the Adjoint Solver and the RBF morph. The approach shown here is based on the use of the Adjoint solver to drive the shape modification of the considered geometry: the adjoint sensitivities are used to guide intelligent design modifications and improve the product perfomance. The presence of geometrical uncertainties is handled using the RBF morph that combines a very accurate control of the geometrical parameters with an extremely fast mesh deformation: a system of radial functions is used to produce a solution for the mesh movement/morphing, from a list of source points and their displacements. An industrial application is presented to show that the Adjoint solver can be used for optimization of a Formula 1 front wing, taking into account the geometrical uncertainties associated with the rotating rubber tire and vehicle steering.

1 Introduction

This work is motivated by the heightened interest in uncertainty quantification of numerical simulations in recent years and, as a consequence, by the interest in a procedure of optimization under uncertainty. One of the objectives of this work is

G. Petrone
Aerospace, Automotive and Turbo CFD Team, ANSYS UK Ltd, Sheffield Business Park, 6 Europa View, Sheffield, S9 1XH, UK, e-mail: giovanni.petrone@ansys.com

D.C. Hill
ANSYS Inc.,10 Canvedish Court, Centerra Resource Park, Lebanon, NH, 03766, USA, e-mail: chris.hill@ansys.com

M.E. Biancolini
Department of Mechanical Engineering, Tor Vergata University, Rome, ITALY, e-mail: biancolini@ing.uniroma2.it

to create a tight coupling between the different optimization modules of ANSYS Fluent[1] in order to challenge shape optimization problems characterized by geometrical uncertainties.

Performing optimization and uncertainty analysis in presence of a large number of design and uncertain variables is a key challenge and the pacing item for the deployment of the proposed methodology based on the use of Adjoint solutions. Petrone et al.[19, 3] optimized the shape of a F1 wheel assembly and proved the necessity of taking account of the uncertainties from the definition stage of the optimization procedure. Nevertheless the genetic algorithm driven optimization under uncertainty and the need to prescribe deformation guidelines during the definition stage of the optimization problem lead to important problems. Above all, the cost of heuristic optimization techniques in robust design is high and their application in the industrial community is still prohibitive. Additionally the need to prescribe "a-priori" deformation guidelines results in a limiting factor when exploring the design space to obtain design solutions that can have a breakthrough impact on the related industry.

For these reasons in this work we assess the use of the Adjoint Solver[11, 2] to guide a robust optimization problem in order to i) reduce the computation effort required by the exploration of the design space, ii) explore non-intuitive design solutions and iii) use combinations of the sensitivity fields to take account of the uncertainties involved in the problem.

2 Optimization Under Uncertainty

Let's consider an objective function in the form $f(z,\xi)$ where $z \in Z$ represents a design variable and $\xi \in \Omega$ represents the input uncertainty. It is possible to introduce an operator Φ, applied to $f(z,\xi)$ in order to obtain a real-valued attribute of it. Considering this assumption, a problem of optimization under uncertainty reduces to the problem of finding $\bar{z} \in Z$ such that

$$\Phi(f(\bar{z},\xi)) \leq \Phi(f(z,\xi)) \;\; \forall z \in Z \tag{1}$$

Different definition for Φ might be used, for example $\Phi(f(z,\xi))$ are the statistical moments of f. The simplest choice is obviously the expected value of f (referred to as **Mean Value Optimization**):

$$\Phi\left(f(z,\xi)\right) = \int_{\Omega} f(z,\xi)\Psi_{\xi} d\xi = \mu(z) \tag{2}$$

where Ψ_{ξ} is the probability density function of ξ. This method is widely used, mostly because the mean is the faster converging moment and relatively few samples are required to obtain a good estimate. Often, however, the mean alone is not able to capture and represent satisfactorily the uncertainties embedded in a given design optimization problem. To overcome this drawback, a possible approach is

the introduction in the objective function of penalization terms that are function of higher order moments (**Mean Value Penalty Optimization**):

$$\Phi\left(f(z,\xi)\right) = w_1\mu(z) + \left(\sum_{k=2}^{N} w_k m^k\left(f(z,\xi)\right)\right)^{1/2} \tag{3}$$

where $w_1,...,w_N$ are (tunable) weights, N is the maximum order of statistical moments considered and $m^k\left(f(z,\xi)\right)$ is the k-th order moment of $f(z,\xi)$. This leads to (for $w_1 = w_2 = 1$ and $N = 2$)

$$\Phi\left(f(z,\xi)\right) = \mu(z) + \sigma(z) \tag{4}$$

where $\sigma^2(z)$ is the variance of $f(z,\xi)$. In this case the optimization under uncertainty seeks to minimize the mean plus standard deviation, giving a formal and mathematically sound construction for the idea of insensitive design.

Another possibility is the **Minimax criterion**[21], very popular in statistical decision theory, according to which the worst case due to uncertainty is the objective for the optimization. This ensures protection against worst case scenario, but it is often excessively conservative.

A popular approach is the **Constrained Optimization**[14], formulated to find $\bar{z} \in Z$ such that

$$\begin{cases} \mu(\bar{z}) \leq \mu(z) \;\; \forall z \in Z \\ \text{s.to:} \qquad\qquad m^k\left(f(z,\xi)\right) \leq C_k \;\forall k \in 2,N \end{cases} \tag{5}$$

where C_k is a constraint on the the order k central moment of $f(z,\xi)$. It easy to notice, as drawback, that the constraint could not be feasible.

The **Multi-objective Approach**[20] is also widely adopted. Here different statistical moments are used as independent tradeoff objectives. In this case a challenge is posed by the increase in the dimensionality of the Pareto front when several statistical moments are used. The research related to the multi-objective method has led to several extensions of the classical Pareto front concept [6, 8, 9, 10, 12, 22, 19].

3 Optimization under uncertainty of a NACA 0012 airfoil

In this section different methodologies for optimization under uncertainty will be used to optimize the shape of a NACA 0012 airfoil using the Fluent AS, starting from a deterministic optimization (i.e. neglecting the presence of uncertainties) used as reference result. The importance of taking in account uncertainty in the optimization of airfoil shape has been addressed in different aerospace and renewable energy studies[15, 16, 17].

The proposed optimization procedure aims to define a general workflow that will be generalized for the more complex applications presented in next sessions of this paper. Even if in aerospace applications the angle of attack is a design condition and

not an uncertainty, in this study it will be assumed as uncertainty to pave the way for the F1 application proposed in the next section. The realizable k-ε turbulence model has been adopted in this study. The FLUENT coupled solver has been preferred to the segrated solver and second order upwind discretization has been chosen for flow and turbulence equations discretization. The velocity magnitude considered in this test case is $100\,m/s$ and, in deterministic conditions, the angle of attack equals 1.55^o. The turbulence intensity has been assumed to be 1% and the turbulent viscosity ratio to be 1. The contour of the pressure flow field around the baseline NACA 0012 airfoil has been show in Figure 3(a) as refence result.

3.1 Deterministic optimization

In this section the Fluent AS is used to guide intelligent design modifications to the baseline case when the uncertainties are not considered in the design procedure. This preliminary study is aimed to assess the ability of the AS to provide a series of design modifications to improve the airfoil performance in terms of efficiency, at a given angle of attack. The deterministic optimization problem is stated as finding $\overline{z} \in Z$ such that

$$\begin{cases} \frac{L}{D}(\overline{z})\big|_{\alpha=\hat{\alpha}} \geq \frac{L}{D}(z)\big|_{\alpha=\hat{\alpha}} \quad \forall z \in Z \\ \text{s.to:} \\ c(z) = c_0 \end{cases} \tag{6}$$

where L is the lift force, D is the drag force, α is the angle of attack, $c(z)$ is the airfoil chord, $\hat{\alpha} = 1.55^o$ and c_0=1 m. The prodecure adopted to perform the deterministic optimization the Fluent AS is described in Figure 1(a).

1. CONTROL VOLUME DEFINITION. A control volume is defined enclosing the initial geometry to be optimized. A grid of control points is superimposed over the mesh in order to facilitate the mesh morphing: moving these control points causes the mesh to smoothly morph by relating them to the grid nodes using Bernstein polynomials. The number of control points has been chosen to be 30 in x direction and 20 in y direction. The morhping box ranges beween -0.3 m and 1.3 m in x direction and between -0.3 m and 0.3 m in y direction.
2. CFD SOLVER CONVERGENCE. A converged CFD solution is evaluated.
3. ADJOINT SOLVER CONVERGENCE. The adjoint solver is converged for the chosen observables (e.g. efficiency), in the same fashion of a CFD solver (i.e. residual based convergence, see Figure 2(a)) and the sensitivies are evaluated.
4. MORPHING. The optimal displacement found by the AS are smoothed and used to morph the geometry via the defined array of control points.
5. ENFORCING CONTRAINTS. Since the legality box chosen in this application doesn't touch the boundaries of the aifoil, during the optimization procedure it could be possible that the chord of the airfoil is reduced or increased by the AS. The choice of a relatively large morphing box in the AS is justified by the

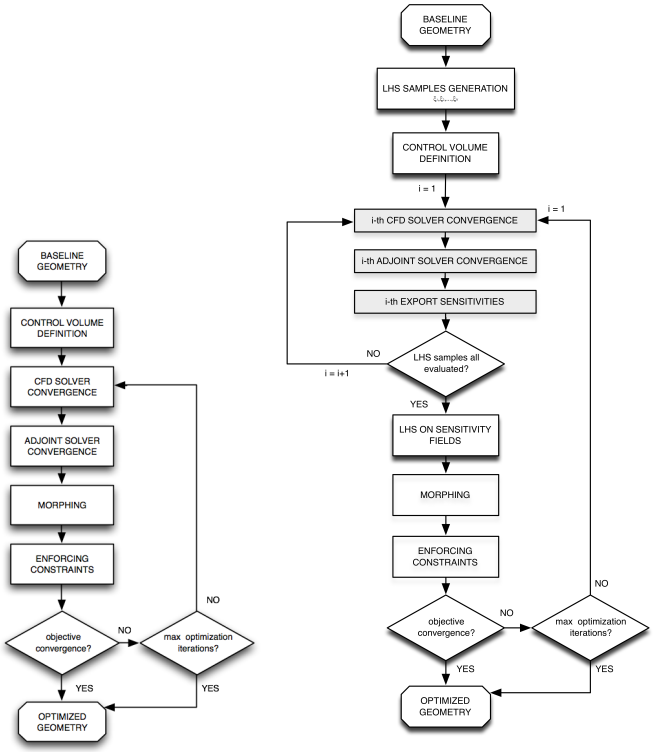

(a) deterministic optimization (b) probabilistic optimization

Fig. 1 Flowcharts of the optimization procedures using Fluent AS

necessity to not freeze the deformations of surfaces that lie on its boundaries, enhancing the exploration of the design space and avoiding an over-constrained optimization problem. To prevent the optimization result from this scenario, a check of the airfoil length is performed after each design modification. In the case that the airfoil length is altered by the morphing, a coherent scale of the mesh is perfomed to balance this effect and recover the original dimension.

6. All the steps 2-5 are repeated in a series of design modifications until the global optimum of the optimization problem is reached and the final design is obtained.

The contour of the pressure flow field around the optimized airfoil has been reported in Figure 3(b). The convergence history of the airfoil efficiency is reported in Figure 5(a). It is possible to notice that the AS is able to produce a monotonic increase of the objective function in each stage of the optimization procedure by successfully driving it.

Comparing Figures 3(a) and 3(b) it is possible to notice that the Fluent AS has morphed the baseline airfoil in order to enhance the velocity expansion on its upper surface, resulting in a particular distribution of the camberline and thickness that had

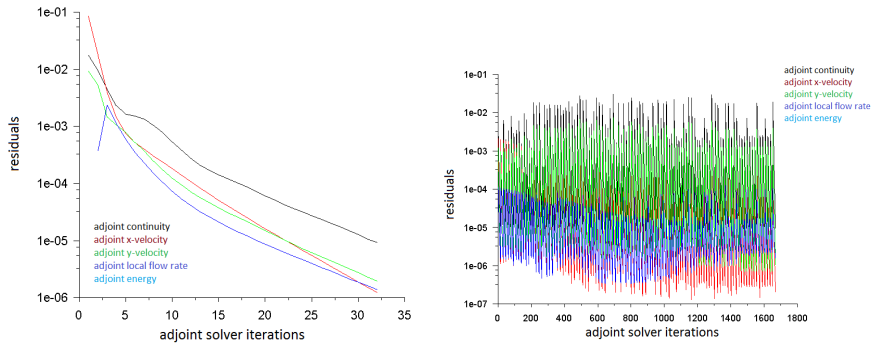

(a) baseline geometry (b) 105 design optimization stages

Fig. 2 Residual convergence of the Adjoint Solver

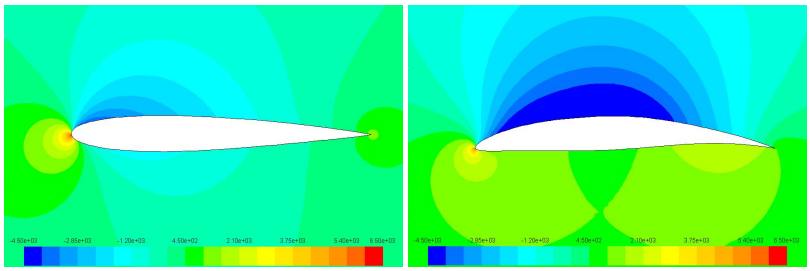

(a) NACA 0012 (b) deterministic optimization

Fig. 3 Pressure distribution at α=1.55^o

been difficult to predict from the defition stage of the optimization procedure. The resulting lift to drag ratio of the optimized airfoil is 58.04, compared to the starting value of 12.11.

In the next sections the first two statistical moments, indipendently and in their combination, will be used to take in account uncertainty in the design procedure.

3.2 Mean Value Optimization

In this section the angle of attack, previously fixed as design condition, is assumed to be an uncertain variable. We represent the uncertainty as purely stochastic, i.e. a measure of variability and our goal is to establish quantitatively its effect on the optimization procedure. A uniform distribution has been assumed for α, with -1.55^o and 5^o respectively as lower and upper bounds. Latin Hypercube Sampling (LHS) [25], a stratified-random procedure which provides an efficient way of sampling

variables from their distributions, has been used to propagate the input uncertainty into the QoI.

The computational procedure is obviously modified by the presence of uncertainty, as shown in Figure 1(b). The Mean Value optimization problem is stated as finding $\bar{z} \in Z$ such that

$$\begin{cases} \mu(\frac{L}{D}(\bar{z},\alpha)) \geq \mu(\frac{L}{D}(z,\alpha)) \ \ \forall z \in Z \\ \text{s.to:} \\ c(z) = c_0 \end{cases} \tag{7}$$

where $\mu(\frac{L}{D})$ is the expected value of the efficiency and α =U[-1.55^o,5^o] is a uniform distribution of the angle of attack. 20 LHS samples have been used to evaluate the mean efficiency in each stage of the optimization procedure. The results of the two optimization procedures differ most in the leading edge and the lower part of the airfoil section. Additionally the mean value optimized airfoil results to be slightly thicker than its deterministic counterpart. The contour of the pressure flow field around the optimized airfoil has been reported in Figures 4(a), 4(g) and 4(m) at 3 different angles of attack, corresponding to 3 LHS samples.

3.3 Variance Optimization

In the previous section the AS was used to obtain the best mean efficiency in correspondence of the prescribed distrution of the angle of attack. In this section, instead, the variance of the efficiency is considered as objective. By minimizing the variance of the efficiency the AS seeks to guarantee a stable value of the performance among all the possible flow conditions, without caring for its actual value. The Variance based optimization problem is stated as finding $\bar{z} \in Z$ such that

$$\begin{cases} \sigma^2(\frac{L}{D}(\bar{z},\alpha)) \leq \sigma^2(\frac{L}{D}(z,\alpha)) \ \ \forall z \in Z \\ \text{s.to:} \\ c(z) = c_0 \end{cases} \tag{8}$$

The contours of the pressure flow fields have been reported in Figures 4(b), 4(h) and 4(n).

3.4 Mean Value Penalty Optimization

In this section the mean and the standard deviation of the efficiency are linearly combined in a unique objective using the Mean Value Penalty approach and the optimization problem is stated as finding $\bar{z} \in Z$ such that

$$\begin{cases} \mu(\frac{L}{D}(\bar{z},\alpha)) - 3\sigma(\frac{L}{D}(\bar{z},\alpha)) \leq \mu(\frac{L}{D}(z,\alpha)) \\ \qquad\qquad -3\sigma(\frac{L}{D}(z,\alpha)) \quad \forall z \in Z \\ \text{s.to:} \\ c(z) = c_0 \end{cases} \tag{9}$$

The contours of the pressure flow fields have been reported in Figures 4(c), 4(i) and 4(o).

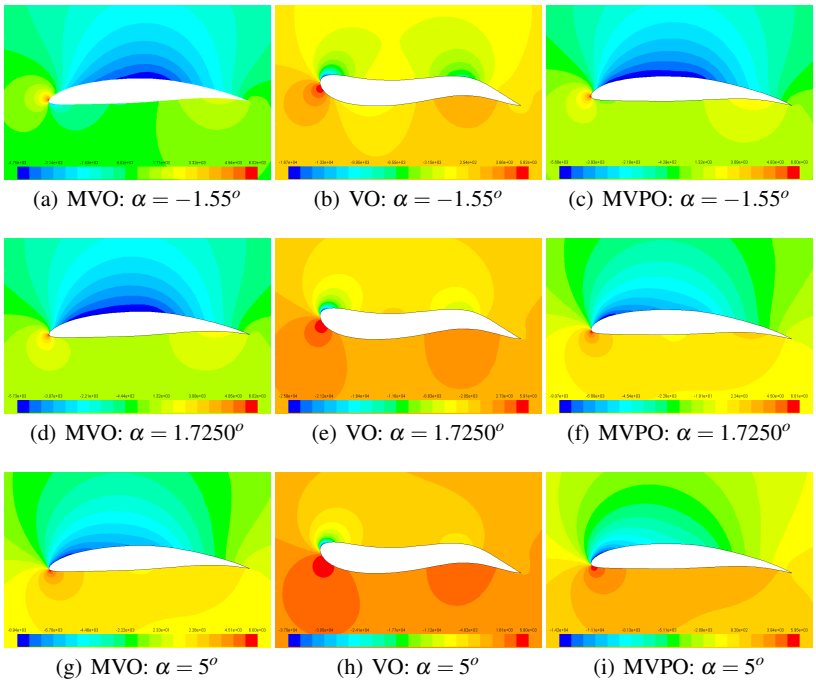

(a) MVO: $\alpha = -1.55^o$ (b) VO: $\alpha = -1.55^o$ (c) MVPO: $\alpha = -1.55^o$

(d) MVO: $\alpha = 1.7250^o$ (e) VO: $\alpha = 1.7250^o$ (f) MVPO: $\alpha = 1.7250^o$

(g) MVO: $\alpha = 5^o$ (h) VO: $\alpha = 5^o$ (i) MVPO: $\alpha = 5^o$

Fig. 4 Airfoil optimization under uncertainty

3.5 Analysis under uncertainty

In this section ANSYS DesignXplorer (DX) has been used to propate the input uncertainty in the QoI by using LHS. The Six Sigma Analysis component of ANSYS DX has been used to evaluate the Probability Density Function (PDF) of the airfoil efficiency, as shown in Figure 6(a). The PDFs of the efficiency for the NACA 0012 and the optimized airfois have been reported in Figure 6(b).

It is possible to notice that the NACA 0012 efficiency (black) shows a quite uniform distribution with a very high variance. This means that values of the efficiency of -10 and 30 are almost equiprobable. The deterministic optimization (DO) solu-

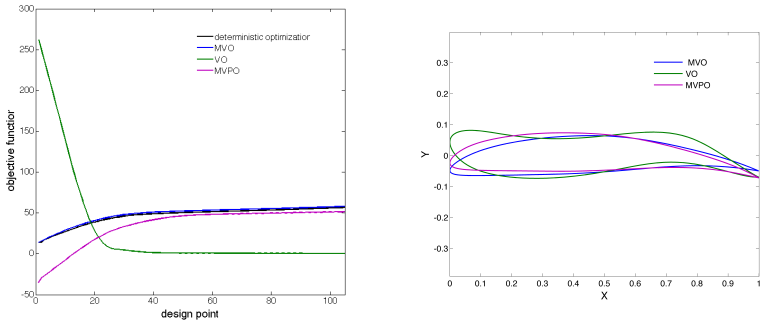

(a) convergence histories (b) airfoil shapes

Fig. 5 Comparison of the optimization methodologies

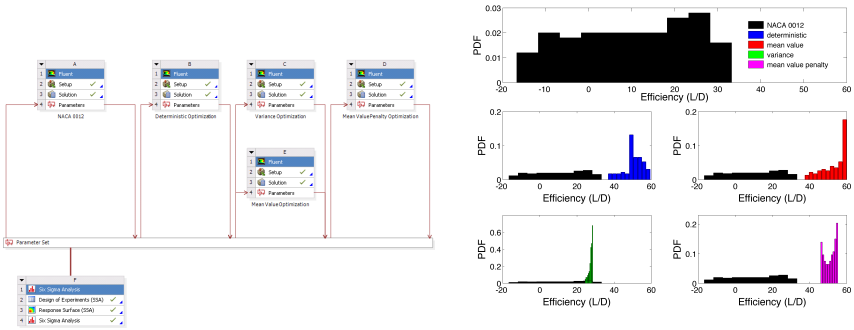

(a) ANSYS DX (b) PDFs of the QoI

Fig. 6 Analysis under uncertainty

tion (blu) results to be not only, in average, more efficient but also more robust with respect to the uncertainty, as shown by the reduced extent of its support. When the mean value otpimization (MVO) is used (red), on one hand the mean efficiency is maximized and it is possible to notice that the distribution becomes more peaked toward higher values of the performance. On the other hand the variance increases since it has not been considered in the formulation of the optimization problem. If the variance optimization (VO) is considered (green), the resulting PDF is almost deterministic (e.g. delta dirac function), being almost insensitive to the angle of attack but showing a reduced average performance.

Finally when the mean value penalty optimization (MVPO) is used a trade-off solution (magenta) between the maximization of the mean efficiency and the minimization of the variance it is obtained. The resulting solution appears to have a slightly higher mean efficiency than that obtained with the deterministic case, but

with a great improvement of the variance. The first four statistical moments of the efficiency have been reported in Table 1 for all the obtained configurations.

Table 1 airfoil efficiency statistical moments

	NACA 0012	DO	MVO	VO	MVPO
μ	12.43	51.40	56.30	27.56	51.97
σ^2	184.96	25.10	38.56	0.98	8.88
γ_1	-0.16	-0.63	-0.91	-1.26	-0.30
κ	1.19	0.02	-0.43	0.83	1.37

4 Optimization under Uncertainty of a F1 front wing assembly

In this section we apply the devoped framework for optimization under uncertainty to the computational design of a Formula 1 front wing assembly using large-scale, three-dimensional Reynolds-Averaged Navier-Stokes simulations. The purpose of designing the front wing is to increase the downforce while minimizing the total drag of the assembly.

Previous studies on a similar F1 assembly[19] showed that the uncertainties that have a significant impact on the Drag force predicition are the tire yaw angle and the inlet conditions: in order to obtain a robust design of the front wing the optimization procedure needs to account for uncertainties arising from variables in flow conditions as well as from variability in the flexible tire geometry. This baseline geometry consists of 10 million polyhedral mesh cells.

RBF Morph[7] is used to generate multiple CFD mesh model variants, while keeping CAD and grid generators out of the design process loop, thus substantially saving design time and costs. The generated models are then used to compute the flow field around the F1 front wing assembly using Fluent.

The discretization schemes of the URANS equations for momentum and turbulence quantities were initially set to first order and then switched to second order for all quantities including turbulent scalars. Once the flow settled into a regular oscillating pattern, time averaging of flow statistics was turned on. The solution was deemed to be converged when the mean flow statistics no longer changed with additional iterations and all the residuals were below the value of $1e^{-5}$. Literature studies[4, 5] where LES was used to predict the flow field around a rotating F1 wheel assembly have shown structures like the horseshoe vortex and secondary flow vortices that are not represented by RANS turbulence closures. These works demonstrated that among the URANS models the Realizable k-ε turbulence model is the most accurate at predicting the vortex eccentricity, therefore it has been adopted in this study.

4.1 Data assimilation

The Monza circuit is reported in Figure 7(a), where the typical speeds in different locations of the tracks have been highlighted together with the adopted gear. With the long straights forming a significant aspect of the Monza circuit layout minimising drag is an important consideration. Even if, for this reason, in F1 industry usually a Monza-only low drag and low downforce front wing is produced, in this work we look for a design of the front wing that seeks to balance between two trade-off objectives: i) drag minimization and ii) downforce maximization. The QoI to maximize is assumed to be the ratio of the downforce to drag, while in future works these objectives will be handled separately.

Lower and upper bounds on the steering angle have been assumed respectively as 0^o and 15^o, while lower and upper bounds on the velocity have been assumed respectively as $22.35m/s$ and $88.51m/s$. The track has been subdived in 11 segments and for each segment a Normal distribution has been considered to model the probability distribution of the velocity and steering angle. The mean of each velocity distribution has been assumed as the typical speed in that part of the track, while the standard deviation has been assumed to be 10 percent of this value. The mean steering angle has been assumed equal to 0 degrees when the gear adopted is the 7th, 3 degrees when the gear adopted is the 6th, 5 degrees when the gear adopted is the 5th, 10 degrees when the gear adopted is the 4th and 15 degrees when the gear adopted is the 3rd and the 2nd. The standard deviation of the steering angle has been always assumed to be 1.5 degrees. A number of Monte Carlo (MC) points equal to $3.5e^6$ have been sampled along the track. For each segment of the track the fraction of points sampled was equal to the ratio between the length of the segment and the length of the circuit (5.793 km for 1 lap). The obtained joint probability of the input uncertainties has been reported in Figure 7(b). It is possible to notice that this joint probability reflects the realistic situation where high velocities - low steering angles and low velocities - high steering angles are encountered during the race.

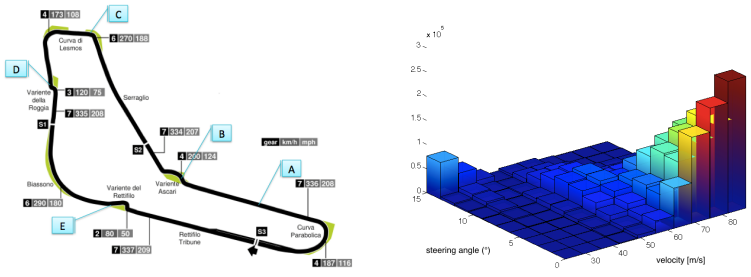

(a) Monza circuit (b) Input joint probability

Fig. 7 Autodromo Nazionale Monza

4.2 Uncertainty propagation

In this section Simplex Stochastic Collocation (SSC)[23, 24] has been used to propagate the input uncertainty into the QoI. Indeed SSC combines the effectiveness of random sampling in higher dimensions with the accuracy of polynomial interpolation. It also leads to the superlinear convergence behavior of Stochastic Collocation methods and the robustness of MC approaches. SSC discretizes the parameter space Ξ using non-overlapping simplex elements Ξ_j from a Delaunay triangulation of sampling points, with $\Xi = \bigcup_{j=1}^{n_e} \Xi_j$, where n_e is the number of elements. In each of the simplexes Ξ_j, the response surface of the quantity of interest, $u(\xi)$ as function of the n_ξ random parameters $\xi \in \Xi$, is approximated by a polynomial $w_j(\xi)$

$$w_j(\xi) = \sum_{m=0}^{P} c_{j,m} \Psi_{j,m}(\xi), \tag{10}$$

with $P+1$ coefficients $c_{j,m}$ and basis polynomials $\Psi_{j,m}(\xi)$. The polynomials are found by interpolation of the samples $v_k = u(\xi_k)$ at the vertexes ξ_k of the simplex elements, with $k = 1, \ldots, n_s$, where n_s is the number of samples. In previous studies on wind turbines simulations[15, 16, 17] , both LHS and SSC outperformed classical MC and it has been proved that the SSC approach leads to stable statistics requiring only a few dozen CFD simulations. Due to these considereations 10 SSC points have been used to propagate the input uncertainty into the QoI.

4.3 Vehicle steering using RBF Morph

The mesh of the steered vehicle can be easily obtained thanks to an advanced feature available for the RBF Morph software. A complex sequence of RBF mesh morphing comprised of four steps is used to: i) deform the tire imposing a prescribed amount of lateral slip of contact patch, ii) prescribe a rigid rotation of the overall wheel assembly about the steering axis, iii) re-project the contact patch on the ground, iv) morph the volume mesh with information gathered on all surfaces.

The user can set-up each wheel prescribing steering kinematics (see Figure 8) and threads belonging to the following set: tire, rim, ground, contact patch and fixed. It is interesting to notice that thanks to an accurate calibration of the rule that defines tire flexibility (the angular portion of tire subjected to deformation increases with the value of lateral slip) it is possible to get a realistic behavior for tire deformation.

The contours of the pressure flow field around the front wing assembly has been reported in Figures 11(a), 11(b) and 11(c) at 3 different race conditions, corresponding to 3 SSC samples. The same SSC samples have been reported in figure 7(a) in correspondence of the position on the circuit from where them were sampled. It is possible to notice the effect of vehicle steering on both the left and right front wheels. Every time that RBF Morph is used to deform the wheels additional oper-

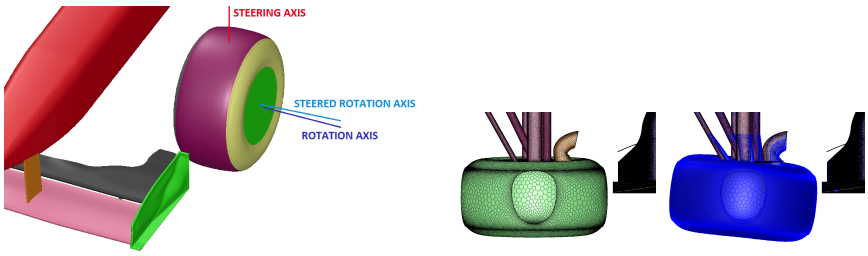

(a) axes definition (b) before steering (c) after steering

Fig. 8 Vehicle steering using RBF Morph

ations are performed to adjust the physics of the simulation: i) the velocity of the inlet and the moving ground are changed to match the velocity and the direction of the SSC sample ii) the rotational speed of the wheels is changed to be coherent with the value of the velocity of the SSC sample and the axis direction is aligned with the steered rotation axis. The SSC statistics reported in Table 2 have been obtained sampling $1e^3$ MC points on the responce surface obtained with equation 10.

4.4 Manipulating adjoint sensitivies

A control volume is defined enclosing the initial geometry to be optimized. The number of control points has been chosen to be $N_x = 30$ in x direction, $N_y = 30$ in y direction and $N_z = 15$ in z direction. The morphing box ranges beween -0.95 m and 0.35 m in x direction, between -0.8 m and 0.8 m in y direction and between -0.066 m and 0.264 m in z direction as shown in Figure 9(a). The resulting number

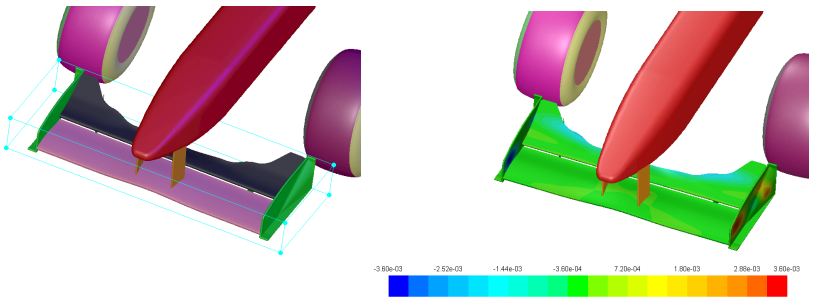

(a) adjoint morphing box (b) normal optimal displacements

Fig. 9 F1 front wing assembly

of control points is $N_{CP} = 1.35e^4$. Given a control point, $CP(x,y,z)$, the AS is able

to estimate the sensitivities, $s^x(x,y,z), s^y(x,y,z), s^z(x,y,z)$, of the objective function to its movement for a given flow condition (i.e. SSC sample). Indeed the shape sensitivity found with the AS is smoothed on the grid of control points, resulting in a sensitivity in x,y and z direction for each one of them. These control points sensitivities are manipulated according to the following procedure.

1. The AS is converged for the k-th of the n_s SSC samples and the control points sensitivities, $s^x_k(x,y,z)$, $s^y_k(x,y,z)$, $s^z_k(x,y,z)$, are exported.
2. For each control point the $s^x_k(x,y,z), \forall k \in [1,n_s]$ are used as objective realizations at SSC samples to reconstruct the response surface $s^x_j(x,y,z,\xi)$ in the same way it was done for the objective function in Equation 10. The same procedure is repeated for the y and z components of the control points sensitivities.
3. For each control point the previously evaluated response surfaces are used to extimate the mean, $\mu_{s^x}(x,y,z)$, $\mu_{s^y}(x,y,z)$, $\mu_{s^z}(x,y,z)$, and the variance, $\sigma^2_{s^x}(x,y,z)$, $\sigma^2_{s^y}(x,y,z)$, $\sigma^2_{s^z}(x,y,z)$, of all the sensitivity components. As it is possible to notice this operation reduces the dependency on the uncertain variables, ξ.
4. For each control point a linear combination of the mean and the standard deviation is derived, e.g. $\mu_{s^x}(x,y,z) - 3\sigma_{s^x}(x,y,z)$. The resulting field is considered as a probabilistic sensitivity field.
5. The probabilistic sensitivity field is imported and used to morph the geometry.

The steps 3-5 are performed externally to ANSYS Fluent. In order to preserve the symmetry of the front wing, the control points sensitivities were exported defining a symmetry plane. In this way the control points sensitivities that are evaluated on the left part of the front wing and copied and installed to the right part as if a mirror plane lies at the mid-point of the control volume.

This procedure aims to adopt the MVPO methodology by not operating directly on the objective, that would require an appropriate adjoint equation to be derived and solved, but on the control point sensitivities.

4.5 Mean Value Penalty Optimization

The normal optimal displacements have been reported in Figure 9(b) for the baseline design Monza-A. The AS is suggesting to pull out the surfaces in correspondence of the red regions and to push in the surfaces in correspondence of the blue regions in order to improve the design performance. This field eliminates the component of the optimal displacement vector that lies in the plane of the wall and gives an indication on the morphing that will be applied when moving the control points to improve the design performance. In the proposed probabilistic framework any SSC sample suggests a particular direction for the morphing, as shown in Figure 9(b), and the effective deformation is obtained manipulating all the information obtained all over the samples.

The result of the morphing procedure has been reported in Figure 10, where it is possible to appreciate the main differences between the baseline (see 10(a)) and

optimized configurations highlithed in the boxes A-F (see 10(b) and 10(c)). The PDFS of the QoI have been reported in Figure 10(d). It is possible to notice how the optimized design is skewed toward highest performances with a reduced low tail probability. This observation is confirmed by the values of the statistical moments reported in Table 2. The contour of the pressure flow field around the optimized configuration has been reported in Figures 11(d), 11(e) and 11(f), in comparison with the baseline configuration at 3 different race conditions, corresponding to 3 SSC samples.

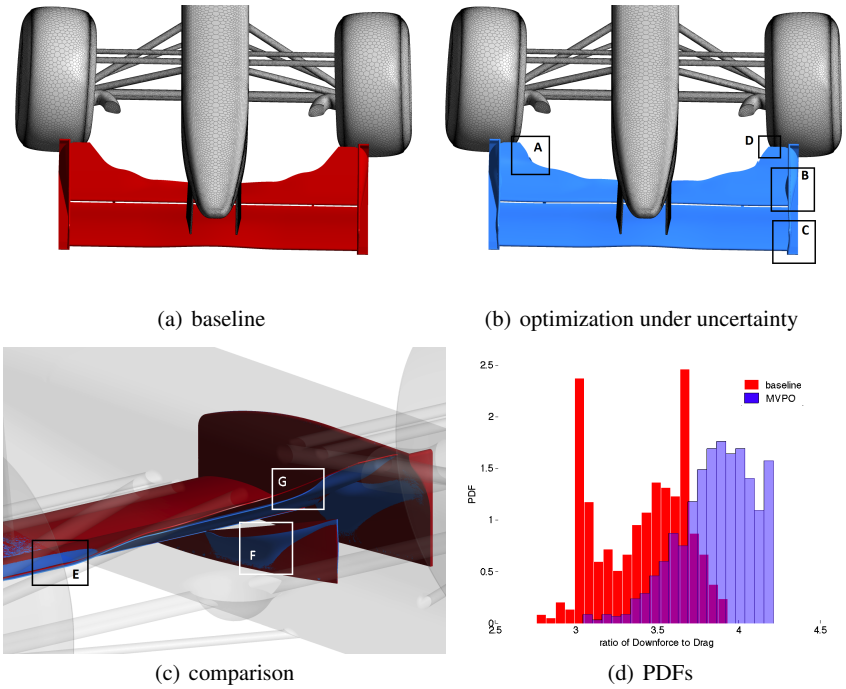

(a) baseline (b) optimization under uncertainty

(c) comparison (d) PDFs

Fig. 10 F1 front wing assembly optimization under uncertainty

Table 2 SSC statistics

	μ	σ^2	γ_1	κ
baseline geometry	3.4012	0.0748	-0.2523	1.8316
MVPO	3.8557	0.0521	-0.6645	3.28

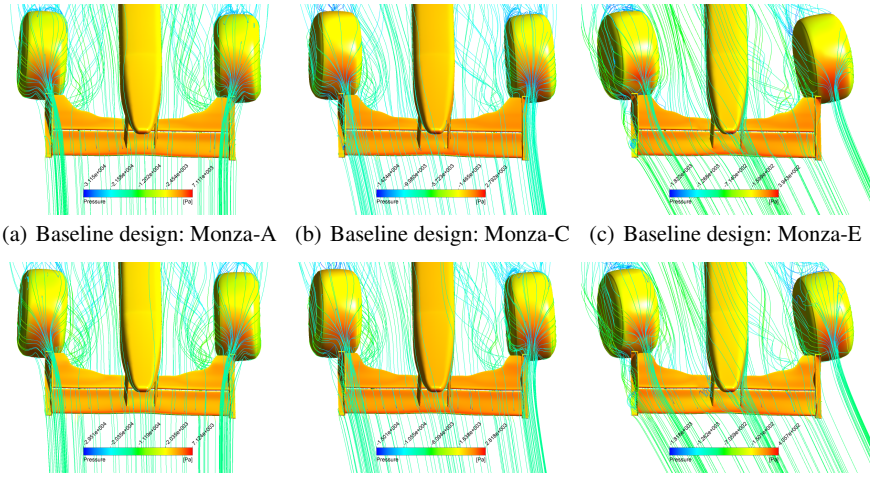

(a) Baseline design: Monza-A (b) Baseline design: Monza-C (c) Baseline design: Monza-E

(d) MVPO: Monza-A (e) MVPO: Monza-C (f) MVPO: Monza-E

Fig. 11 Contours of the flow field around the baseline and optimized F1 front wing assembly

5 Conclusions

In this work we proposed a procedure to perform optiimazation under uncertainty using the sensitivities obtained with the Fluent Adjoint Solver. We expect this aspect of the method to have the most impact because of the generality of the idea, the broad applicability and the opportunity to tackle robust design in a fundamental new way from an industrial perspective. The Formula 1 application shows the importance of taking into account uncertainties from the beginning of the design process. Additionally using the same methodology it is possible to design different F1 components based on the characteristics of a particular track. In future works we will address the possibility to integrate the structural deformation of the aerodynamic components in the probabilistic design procedure and to perform multi-objective design optimization under uncertainty.

References

1. ANSYS FLUENT 14.5 - Theory Guide, ANSYS, Inc., Canonsburg, PA, 2012.
2. ANSYS FLUENT 14.5 - Adjoint Solver Module Manual, ANSYS, Inc., Canonsburg, PA, 2012.
3. Axerio, J., Iaccarino, G., Petrone, G., and Sellapan, V., Extreme Ensemble Computation for Optimization Under Uncertainty , Proceedings of EUROGEN2011 Evolutionary and Deterministic Methods for Design, Optimization and Control, Capua, Italy, September 14-16, 2011 (ISBN 978-88-9063-230-3), pp 743-757.
4. Axerio, J.,Iaccarino, G., Asymmetries in the Wake Structure of a Formula1 Tire, Proceedings of the Sixth International Symposium on Turbulence and Shear Flow Phenomena, vol. 2, pp.

523528, Seoul, South Korea, 2009.
5. Axerio, J., Iaccarino, G., Issakhanian, E., Lo, K., Elkins, C., Eaton, J., Computational and Experimental Investigation of the Flow Structure and Vortex Dynamics in the Wake of a Formula 1 Tire, Society of Automotive Engineers, Technical Paper 2009-01-0775, 2009.
6. Basseur, M., Zitzler, E., Handling uncertainty in indicator-based multiobjective optimization. International Journal of Computational Intelligence Research 2(3): 255272, 2005.
7. Biancolini, M.E., Biancolini, C., Costa, E., Gattamelata, D., Valentini, P.P., Industrial Application of the Meshless Morpher RBF Morph to a Motorbike Windshield Optimisation, European Automotive Simulation Conference (EASC), 6-7 July 2009, Munich, Germany.
8. Coelho, E., Bouillard, P., Multi-objective reliability-based optimization with stochastic metamodels. Evolutionary Computation 19(4):525560, 2011.
9. Deb, K., Gupta, H., Introducing robustness in multi-objective optimization. Evolutionary Computation 14(4):463494, 2006.
10. Deb, K., et al., Reliability-based optimization using evolutionary algorithms. Evolutionary Computation, IEEE Transactions on 13(5):10541074, 2009.
11. Hill, D.C., The Automatic Generation of Adjoint Solutions for a General Purpose Flow Solver. 46th AIAA Aerospace Sciences Meeting and Exhibit, vol. AIAA-2008-904, Reno, Nevada (US).
12. Hughes, E., Evolutionary multi-objective ranking with uncertainty and noise. In Evolutionary multi-criterion optimization, pp. 329343. Springer, 2001.
13. Nadarajah, S.K., Jameson, A., A comparison of the continuous and discrete adjoint approach to automatic aerodynamic optimization. 37th AIAA Aerospace Sciences Meeting and Exhibit, vol. AIAA-2000-667, Reno, Nevada (US).
14. Mattson, C. A., Messac, A., Pareto Frontier Based Concept Selection Under Uncertainty, with Visualization. Optimization and Engineering 6(1):85115, 2005.
15. Petrone, G., de Nicola, C., Quagliarella, D., Witteveen, J., Iaccarino, G., Wind Turbine Performance Analysis Under Uncertainty, AIAA. 49th AIAA Aerospace Sciences Meeting Including The New Horizons Forum And Aerospace Exposition. Orlando, 2011 (AIAA-2011-0544), pp 1-18.
16. Petrone, G., de Nicola, C., Quagliarella, D., Witteveen, J., Axerio, J., Iaccarino, G., Wind Turbine Optimization Under Uncertainty with High Performance Computing, 41st AIAA Fluid Dynamics Conference and Exhibit 27 - 30 Jun 2011. Honolulu, Hawaii (AIAA-2011-3806), pp 1-16.
17. Petrone, G., de Nicola, C., Quagliarella, D., Witteveen, J., Iaccarino, G., Optimization of wind turbine performance and noise under uncertainty, Wind Turbine Noise 2011. Rome, 2011 (ISBN 978-88-88942-339) pp 1-16.
18. Petrone, G., Iaccarino, G., Quagliarella, D., Robustness Criteria in Optimization Under Uncertainty, Proceedings of EUROGEN2011 Evolutionary and Deterministic Methods for Design, Optimization and Control, Capua, Italy, September 14-16, 2011 (ISBN 978-88-9063-230-3), pp 586-603.
19. Petrone, G., Axerio, J., Quagliarella, D., Iaccarino, G., A Probabilistic Non-Dominated Sorting Genetic Algorithm for Optimization Under Uncertainty, forthcoming in Engineering Computation (30), vol. 8 , 2013, ISSN: 0264-4401.
20. Poloni, C., Padovan, L. Parussini, L., Pieri, S., Pediroda, V., Robust Design of Aircraft Components: a Multi-Objective Optimization Problem, von Karman Institute for Fluid Dynamics, Lecture Series 2004-07, November 15-19, 2004, ISBN 2-930389-5
21. Tang, Z. et al., Lift maximization with uncertainties for the optimization of high lift devices using Multi-Criterion Evolutionary Algorithms. In IEEE Congress on Evolutionary Computation, pp. 2324-2331, 2009.
22. Teich, J., Pareto-front exploration with uncertain objectives. In Evolutionary multi-criterion optimization, pp. 314328. Springer, 2001.
23. Witteveen, J.A.S., Iaccarino, G., Simplex Elements Stochastic Collocation for Uncertainty Propagation in Robust Design Optimization 48th AIAA Aerospace Sciences Meeting, Orlando, Florida (2010) AIAA-2010-1313.

24. Witteveen, J.A.S., Iaccarino, G., Simplex elements stochastic collocation in higher-dimensional probability spaces, 51st AIAA/ASME/ASCE/AHS/ASC Structures, Structural Dynamics, and Materials Conference, Orlando, Florida (2010) AIAA-2010-2924.
25. Wyss, G.D. and Jorgensen, K.H., A users guide to LHS: Sandias Latin hypercube sampling software, 1998. Available online at: http://www.prod.sandia.gov/cgi-bin/techlib/access-control.pl/ 1998/980210.pdf